



OPEN

Exploring the spatial and seasonal heterogeneity of cooling effect of an urban river on a landscape scale

Wen Zhou✉, Tao Wu & Xin Tao

Urban water bodies can effectively mitigate the urban heat island effect and thus enhance the climate resilience of urban areas. The cooling effect of different water bodies varies, however, the cooling heterogeneity of different sections of a single watercourse or river network is rarely considered. Based on various satellite images, geospatial approaches and statistical analyses, our study confirmed the cooling heterogeneity from spatial and seasonal perspectives of the Suzhou Outer-city River in detail in the urban area of Suzhou, China. The cooling effect of the river was observed in the daytime in four seasons, and it is strongest in summer, followed by spring and autumn, and weakest in winter. The combination of the width of the river reach, the width and the NDVI value of the adjacent green space can explain a significant part of the cooling heterogeneity of the different river sections in different seasons. Land surface temperature (LST) variations along the river are more related to the width of the river reach, but the variations of the cooling distance are more related to the adjacent green space. The cooling effect of a river reach could be enhanced if it is accompanied by green spaces. In addition, the cooling effect of a looping river is stronger on the inside area than on the outside. The methodology and results of this study could help orient scientific landscape strategies in urban planning for cooler cities.

Keywords Urban river, Cooling effect, Spatial heterogeneity, Seasonal variation, Climate adaptation

Along with the rapid urbanization, landscape patterns and material and energy processes in cities have also changed dramatically^{1–4}. The transformation of urban land-use and land cover (LULC) has altered the surface thermal characteristics, and the high concentration of urban population has led to increased heat emissivity and anthropogenic heat production^{5–7}, much of which causes the urban heat island (UHI) effect⁶. The UHI effect is a climatic phenomenon of higher air and surface temperatures in urban areas than in the rural areas surrounding them^{8–10}. In response to the negative impacts of the UHI effect on our living environment, potential mitigation and adaptation strategies are attracting considerable interest^{5,11}.

The cooling effect of urban blue space (areas dominated by surface water bodies) and urban green space (areas dominated by vegetation cover) is increasingly recognized as a promising nature-based solution to alleviate the UHI phenomenon^{12–15}. Urban water bodies can reduce ambient surface/air temperature, and form an “urban cooling island” (UCI) in summer daytime due to the great specific heat capacity and evaporation effect^{16–19}. Through the exchange of air convection, the cooler air originating from an urban water body is transported to the surrounding areas, and the cooling distance can reach 1000 m^{20,21}. However, research on the cooling effect of urban blue spaces is much less than that of green spaces, although they have great cooling potential^{22,23}.

Heterogeneity of the cooling effect existed among different water bodies according to previous efforts. Some studies found little cooling or even warming effect of urban water bodies^{24–26}, but others reported significant cooling effect (up to 5.5 °C)^{16,27,28}. Literature indicates that the magnitude of the cooling effect of urban water bodies is affected by the size, shape, location, surrounding landscape and background climate (e.g., wind speed and direction)^{25,27,29–31}. Specifically, taking 21 water bodies in Shanghai as a case, Du et al.²⁷ found that a simple shape and a lower proportion of surrounding impervious surface resulted in a stronger UCI effect of the water body. Syafii et al.³⁰ demonstrated that larger and more regularly shaped water bodies cause a more significant

College of Horticulture and Landscape Architecture, Yangzhou University, Yangzhou 225000, China. ✉ email: wenzhou0305@hotmail.com

drop in air temperature. Brans et al.²⁵ discovered a warming effect for urban water bodies compared to rural water bodies (up to 3.04 °C).

Based on spatial form, blue space can be broadly categorized into two types: linear watercourses (e.g., rivers and streams) and polygonal water bodies (e.g., lakes, ponds, reservoirs and wetlands). The heterogeneity of cooling effect of different water bodies and the influencing factors have been widely discussed^{28,31,32}. However, much less attention has been paid to the UCI effect of a single watercourse or river system in detail. Many problems remain to be solved. For instance, does the cooling heterogeneity of the different sections of a river network exist? If so, what are the main factors causing this spatial heterogeneity? What type of surrounding landscape has the most significant influence on the UCI effect of a river reach? These uncertainties have limited the ability of urban planners to make specific recommendations to achieve a more significant cooling effect of water bodies, especially in water-rich cities.

Against this background, this study proposed to quantitatively investigate the spatial heterogeneity and seasonal variation of the UCI effect of a major urban river in Suzhou—the Suzhou Outer-city River, and the relationships with the characteristics of different river reaches and surrounding landscape composition. Based on high-resolution Google Earth maps and Landsat-8 satellite imagery, 141 sampling sites were selected along the river with different inner and outer riverside landscapes and characteristics (e.g., width, elevation). Our objective is to: (1) quantify and compare the distributions of mean LST and cooling distances of 141 river reaches; (2) model the relationships between surface temperatures of different river sections and landscape variables; and (3) investigate the spatial heterogeneity and seasonal correlation of cooling distances of 141 river reaches. The landscape indicators selected in this study could help explain a large portion of the spatial variation in surface temperature and cooling distance, and implications for landscape planning for climate adaptation are discussed.

Study area and data

Study area and site description

Suzhou is located in the middle of the Yangtze River Delta in eastern China's Jiangsu Province (Fig. 1a). The Suzhou metropolitan region covers a total area of approximately 8657 km², and had a population of about 12.8478 million in 2021. Suzhou is a top-ranking water-rich Chinese city, with almost 37% of its land area covered by water. The rate of greenery coverage in built-up area of the urban district was 43.29% in 2021³³. The main portion of the city lies on a flat plain with a few remnant hills in the southwest, and the average elevation is 3.5–5 m above sea level. The flow velocity is not greater than 0.1 m/s³⁴, so the flow velocity is not considered in this study. Suzhou is characterized by a north subtropical humid monsoon climate, and had a mean annual temperature of 18.3 °C and a mean annual precipitation of 1318.6 mm in 2021³³. The Outer-city River investigated in this study is a part of the Suzhou river system with approximately 15,400 m long, and is located in Gusu District which is the old town of Suzhou city (Fig. 1b,c).

As can be seen in Fig. 1d, the research path can be simply summarized into two routes, namely the longitudinal route A-A' and the transverse route B-B'. For route A-A', 141 sampling sites were chosen around the centerline along the watercourse from the starting point to the ending point in a counterclockwise direction, and designated as Site 1 through Site 141. These 141 sampling sites were selected mainly with respect to their differences in the width of their situated river reaches and LULC types on the riverbanks (inside and outside). Since the spatial resolution of the LST data is 30 m, river reaches with a width of less than 30 m were excluded in this study to ensure that each sample point extracts only the LST value of the water body. The LST of 141 sampling sites for six dates was extracted to analyze their spatial and seasonal variations and the corresponding influencing factors. Unlike route A-A', routes B-B' are cross-sectioned for each sampling site at both the landscape (Fig. 1e) and LST levels to quantify LULC characteristics and transverse LST variations, respectively. More information on route B-B' LST profile is presented in “Quantification of cooling intensity and selection of landscape variables”.

Data descriptions and applications

Data used in this study include six cloud-free Landsat-8 Operational Land Imager (OLI) images with multiple spectral bands with 30-m resolution and one panchromatic band with 15-m resolution, and Thermal Infrared Sensor (TIRS) imagery with 30-m resolution, and six high-resolution Google Earth maps and DEM (Digital Elevation Model, 30-m resolution) data. The OLI data was applied to calculate the NDVI (Normalized Difference Vegetation Index) value. The TIRS data was applied to derive LST data. The Landsat-8 imagery was obtained from the United States Geological Survey (<https://glovis.usgs.gov/>). The detailed imagery information is shown in Table 1. Besides, high-resolution Google Earth maps were used for LULC classification through manual interpretation. DEM data were applied to extract elevation information of various river reaches obtained from the Geospatial Data Cloud website (www.gscloud.cn).

The primary consideration in selecting Landsat 8 imagery was the quality of the imagery. Since the cooling effect of urban water bodies was expected to be most pronounced during the daytime in summer, three Landsat-8 datasets were obtained from summer, and one from each of the other three seasons. The study area was the ancient city of Suzhou Gusu District, whose landscape has hardly changed in recent decades due to the policy of protecting the ancient city of Suzhou.

The LST maps were derived using radiative transfer equation (RTE) method³⁴ and the results of spatial distribution of LST were shown in Fig. 2. The most important steps, for convenience, are shown as follows:

$$L_{\lambda} = m_{\lambda} \times DN + n_{\lambda} \quad (1)$$

where L_{λ} is the sensor radiance converted from the DN value ($W \cdot m^{-2} \cdot sr^{-1} \cdot \mu m^{-1}$); m_{λ} and n_{λ} represent the scale factors obtained from Landsat-8 metadata file; DN represents the digital number value of image pixel.

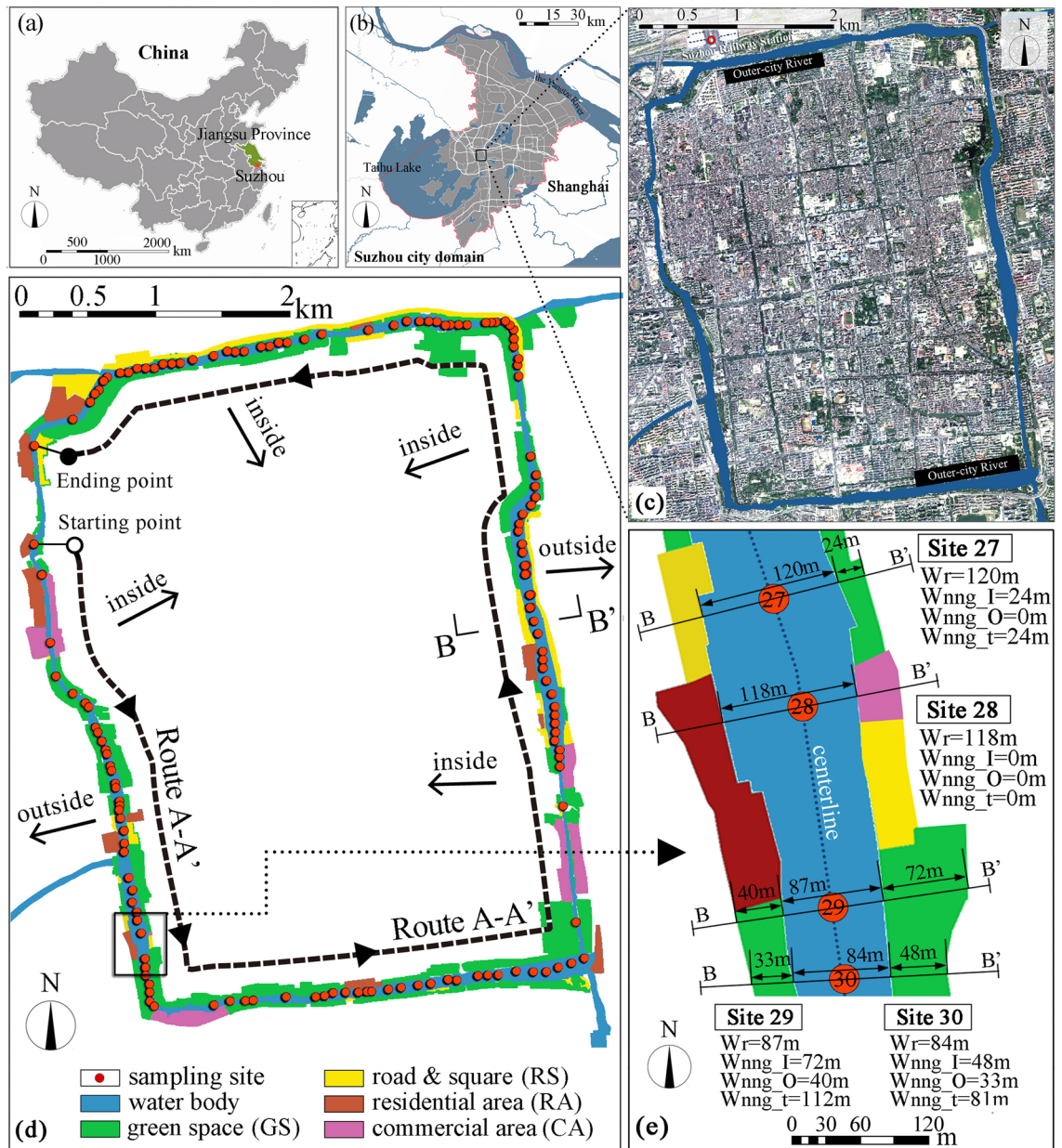


Figure 1. (a). China map and the location of Suzhou city; (b) the location of Suzhou Outer-city river; and (c) satellite imagery of the old town of Suzhou and the Outer-city River marked in dark blue; (d) the location of the 141 sampling sites (numbered 1–141 from the starting point to the ending point) and riverside LULC types; and (e) route B–B’ landscape profiles of Site 27–30 showing the definitions of W_r , W_{nng_I} , W_{nng_O} and W_{nng_t} . W_r is the width of the river reach. W_{nng_I} and W_{nng_O} are the transverse widths of the inside and outside nearest neighbor greenspace. W_{nng_t} is the sum of W_{nng_I} and W_{nng_O} . Here, nng (the nearest neighbor greenspace) refers to the green space that is in direct contact with the river reach.

Seasons	Scene ID	Acquisition date	Acquisition time (BJT)
Summer/hot	LC81190382014203LGN00	22 July, 2014	10:31 am
	LC81190382017147LGN00	27 May, 2017	10:30 am
	LC81190382021174LGN00	23 June, 2021	10:31 am
Spring/warm	LC81190382019105LGN00	15 April, 2019	10:30 am
Autumn/cool	LC81190382019313LGN00	9 November, 2019	10:31 am
Winter/cold	LC81190382021030LGN00	30 January, 2021	10:31 am

Table 1. Descriptions of the Landsat 8 OLI/TIRS images used. *BJT* Beijing time.

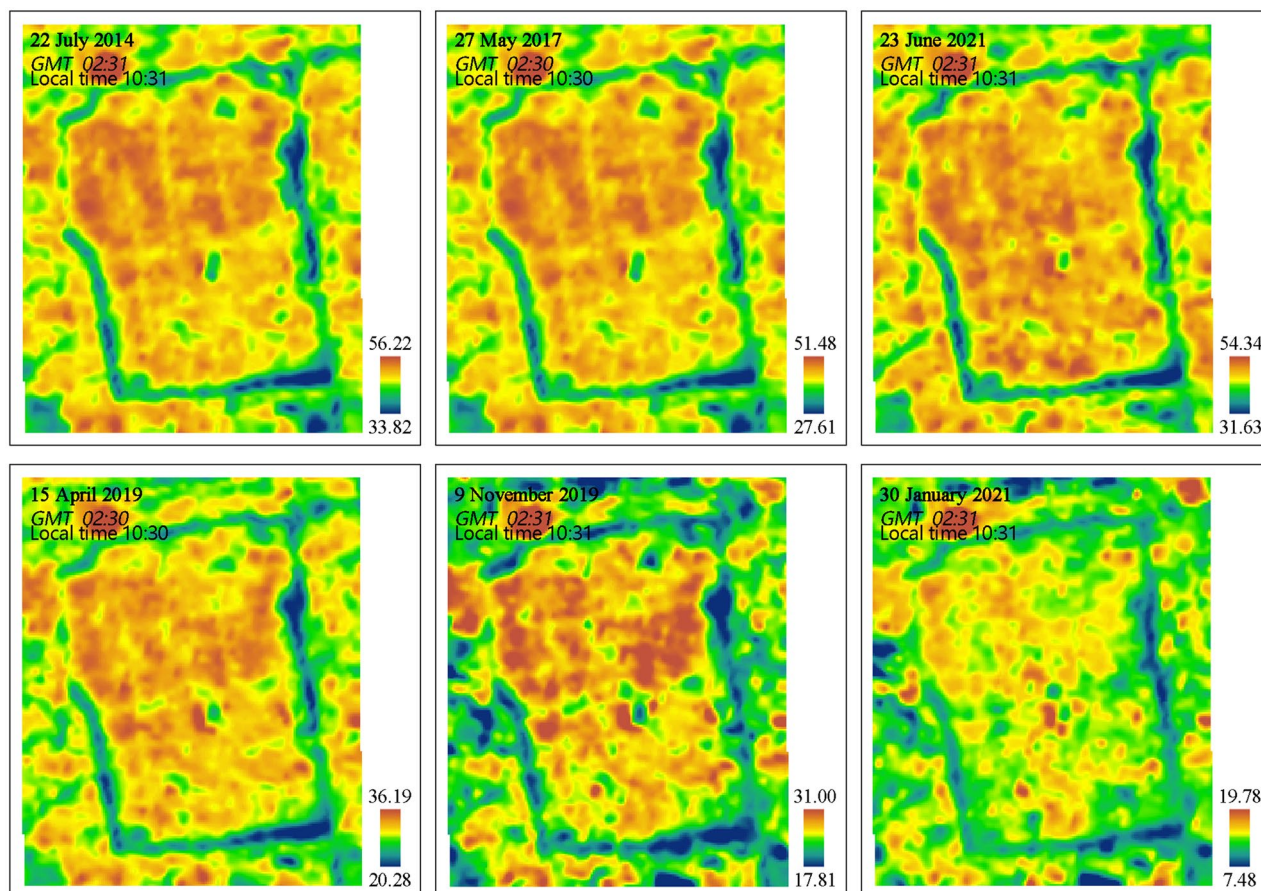


Figure 2. Land surface temperature ($^{\circ}\text{C}$) maps of the six dates.

$$B(T_S) = [L_{\lambda} - L \uparrow - \tau(1 - \varepsilon)L \downarrow] / \tau\varepsilon \quad (2)$$

$B(T_S)$ refers to the ground radiance; ε and τ represent the land surface emissivity and atmospheric transmissivity, respectively; and $L \uparrow$ and $L \downarrow$ are the upwelling and downwelling atmospheric radiances ($\text{W}\cdot\text{m}^{-2}\cdot\text{sr}^{-1}\cdot\mu\text{m}^{-1}$), respectively.

$$T_S = K_2 / \ln(K_1 / B(T_S) + 1) \quad (3)$$

where T_S is the LST; K_1 and K_2 are the calibrated constants with the values of $774.88 \text{ W}\cdot\text{m}^{-2}\cdot\text{sr}^{-1}\cdot\mu\text{m}^{-1}$ and 1321.08 K (i.e., Kelvin degree) for the Landsat 8, respectively.

Method

Quantification of cooling intensity and selection of landscape variables

The mean LST (T_{mn}) and maximum cooling distance (CD) were used to measure the UCI intensity of different reaches along the river, and a lower T_{mn} and a larger CD refer to a stronger UCI effect. Since UCI intensity was always quantified by the temperature difference between the water body and the ambient environment, a higher UCI intensity could be explained by a lower LST of the water body. Specifically, the T_{mn} of a river reach is measured by the LST of the grid cell where the sampling point is located (i.e., the middle grid cell of the river reach). Similar to previous studies^{35–38}, the value of CD for each reach was defined as the distance between the edge of the reach and the first turning point of LST. LST of all grid cells (30 m each) along the transverse route B-B' of the river reach was extracted and prepared to identify the maximum CD (CD_i and CD_o). CD_{mean} is the mean value of CD_i and CD_o of a river reach.

In addition to the characteristics of the water body itself, the magnitude of the cooling effect was also expected to be influenced by the surrounding landscapes. In order to identify the most influential LULC type on the cooling effect of the river, the riverine landscapes were classified into four types: green space (GS), roads or squares (RS), residential area (RA), and commercial area (CA) (Fig. 1d). Each type was further divided into two categories showing location, including green space on the outside (GS_out) and green space on the inside (GS_in), and the same for other LULC types. See Supplementary Fig. 1 for a description of LULC shares across all 141 sampling sites. Based on multiple regression analysis, after LULC types were transformed into dummy variables, the results confirmed the dominant influence of green space (GS_in and GS_out) on the riverbank

among the different LULC types on the UCI effect of the river reach (Supplementary Table 1). This is because vegetated areas are not only associated with a relatively lower air/surface temperature^{39–41}, but can also cool their immediate surroundings^{42,43}. Therefore, a dataset describing the characteristics of river reaches and adjacent GS was prepared. Reach-related descriptors were *Wr* and *Er*; and neighboring vegetation-related descriptors included *Wnng_I*, *Wnng_O*, *Wnng_t*, *NDVI_{inng_I}* and *NDVI_{inng_O}* and *NDVI_{inng_t}*. *NDVI_{inng_I}* and *NDVI_{inng_O}* represent the NDVI of the inner-side and outer-side nearest adjacent green space; and *NDVI_{inng_t}* was the sum of *NDVI_{inng_I}* and *NDVI_{inng_O}*. See Table 2 for definitions of cooling indicators and landscape indicators, and see Fig. 1 (e) for the calculations of landscape indicators in this study.

Analysis process and methods

The dummy variable is used to determine which type of riverbank LULC most affects the cooling intensity and distance of river reach. Bivariate correlation analyses and regression analyses were then conducted to identify and quantify the relationships between the cooling indicators ($T_{mn}/CD_i/CD_o$) and various landscape variables of 141 sampling sites in four seasons, as well as the seasonal relevance. The stepwise multiple linear regression (SW-MLR) method was performed to quantify the effect of selected landscape variables on the cooling effect of 141 sampling sites. The relative weights (RW) analysis method⁴⁴ was then used to derive the predictive power of the landscape variables on the regression models. All statistical analyses were performed using SPSS 23.0 (SPSS Inc., Chicago, IL, USA).

Results

Distributions of UCI intensities and cooling distances of the different river sections

Figure 3 showed the LST profiles along route A-A' and demonstrated that there is spatial heterogeneity in the mean LST (T_{mn}) both existed between 141 reaches and between different seasons. Combined with the values of range and standard deviation, spatial heterogeneity in UCI intensity between reaches was greatest in summer (i.e., July 22, 2014, May 27, 2017, and June 23, 2021), followed by spring, and very small T_{mn} differences were observed in autumn and winter. Besides, T_{mn} of 141 sampling sites in different seasons were characterized by normal distributions. The trends in the LST curves increase and decrease randomly, and no specific patterns were observed for all six dates. It was noteworthy that the peaks and valleys along the LST curves were essentially in the same locations, implying that reaches with higher LST appear to have higher LST at other times and seasons and vice versa.

To further understand the distribution of maximum CD values of the different river sections for different directions and seasons, the cooling distances of the inner (CD_i) and outer (CD_o) sides were summarized in terms of minimum, maximum, range, mean and standard deviation (StdDev) values, as presented in Table 3. The value of CD_i ranged from 18–601 m, 43–550 m, 75–583 m and 40–467 m in summer, spring, autumn and winter, respectively. The value of CD_o ranged from 8–286 m, 62–500 m, 50–396 m and 50–324 m in summer, spring, autumn and winter, respectively. Overall, the maximum, range and mean values of CD_i were all greater than CD_o at different seasons.

The results showed significant differences between CD_i and CD_o ($p < 0.001$) in four seasons. Moreover, most CD_i were obviously greater than CD_o for a single sampling site, especially in summer (Fig. 4). On all six dates, both CD_i and CD_o curves varied arbitrarily, and the peaks and valleys along route A-A' profiles were most likely at the same locations in three summer dates. The positive linear correlations of CD_i/CD_o among the different dates were confirmed by regression analysis ($p < 0.01$), suggesting that the river section with a greater CD always had a greater CD in other seasons, and vice versa (Supplementary Fig. 2). Overall, the results confirmed the spatial heterogeneity of different sections of an urban river and the seasonal stability of fixed river sections on urban cooling.

	Abbreviations	Descriptions
Cooling indicators	T_{mn}	The mean LST of a river reach (°C)
	CD_i	The maximum cooling distance of a river reach in the inward direction (m)
	CD_o	The cooling distance of a river reach in the outward direction (m)
	CD_{mean}	The mean value of CD_i and CD_o of a river reach (m)
Landscape indicators	<i>Wr</i>	The width of the reach (m)
	<i>Wnng_I</i>	The transverse widths of inner-side nearest neighbor greenspace of the reach (m)
	<i>Wnng_O</i>	The transverse widths of outer-side nearest neighbor greenspace of the reach (m)
	<i>Wnng_t</i>	The sum of <i>Wnng_I</i> and <i>Wnng_O</i> (m)
	<i>NDVI_{inng_I}</i>	The NDVI of inner-side nearest neighbor greenspace of the reach
	<i>NDVI_{inng_O}</i>	The NDVI of outer-side nearest neighbor greenspace of the reach
	<i>NDVI_{inng_t}</i>	The sum of <i>NDVI_{inng_I}</i> and <i>NDVI_{inng_O}</i>
	<i>Er</i>	the elevation of the river reach (m)

Table 2. Definitions of cooling indicators and landscape indicators in this study.

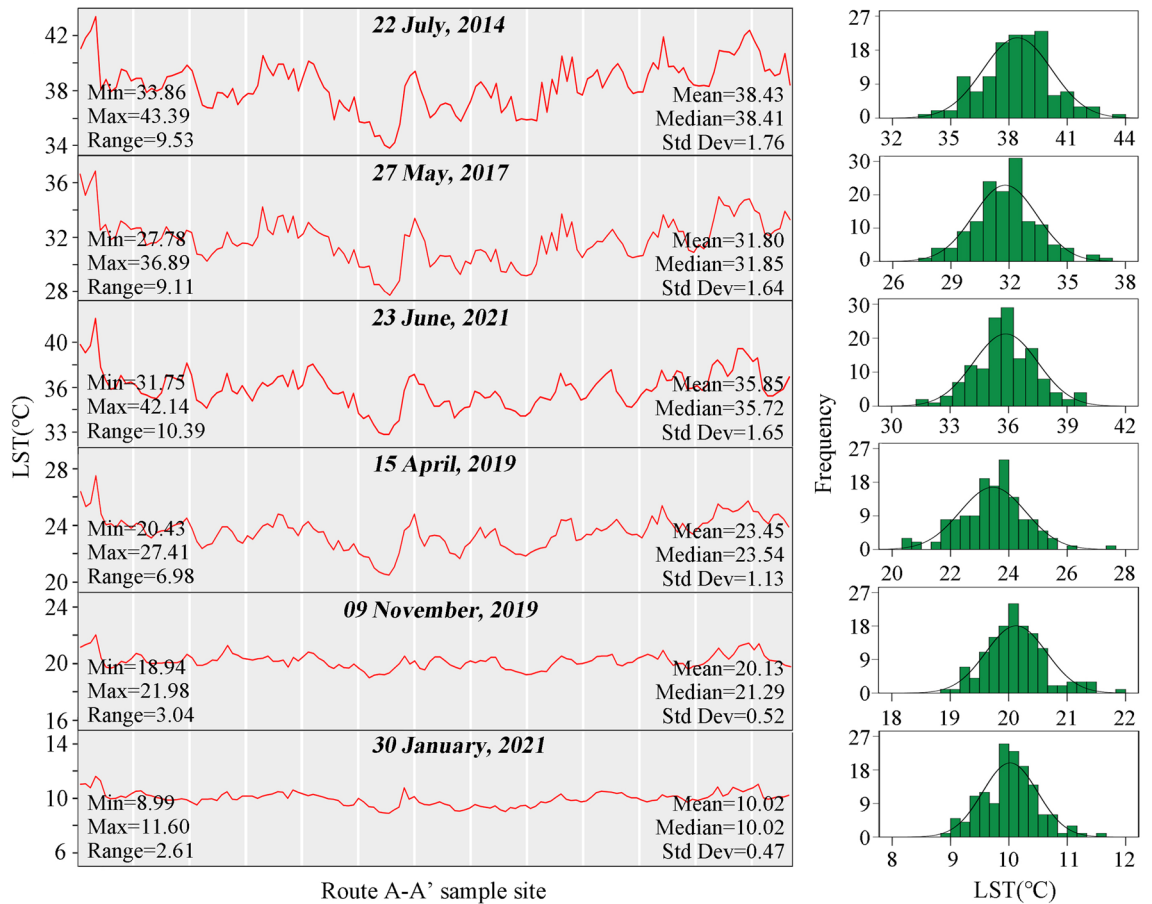


Figure 3. Profiles and distributions of LST (°C) of 141 sampling sites along route A-A' of six dates.

	Min	Max	Range	Mean	StdDev		Min	Max	Range	Mean	StdDev
CD _i _0722	18	512	494	176.9	98.13	CD _o _0722	12	231	219	91.6	40.46
CD _i _0527	33	532	499	190.3	105.5	CD _o _0527	8	250	242	91.25	42.47
CD _i _0623	60	601	541	231.57	113.25	CD _o _0623	54	286	232	151.12	44.38
CD _i _0415	43	550	507	237.12	115.87	CD _o _0415	62	500	438	188.6	103.05
CD _i _1109	75	583	508	228.37	109.26	CD _o _1109	50	396	346	156.3	64.3
CD _i _0130	40	467	427	184.62	93.8	CD _o _0130	50	324	274	140.39	53.63

Table 3. Statistical summary of inside (CD_i) and outside (CD_o) cooling distances for six dates (unit: m). 0722, 0527, 0623, 0415, 1109 and 0130 represent 22 July, 2014; 27 May, 2017; 23 June, 2021; 15 April, 2019; 9 November, 2019 and 30 January, 2021, respectively.

Effects of landscape indicators on the surface temperature of river reaches

Variations in the mean LST (T_{mn}) of different river sections were associated with the scale of the reach and the characteristics of its riverside green spaces (Fig. 5). No correlations were found between T_{mn} and the elevation of reach (E_r) for all seasons. W_r , W_{nmg-t} and $NDVI_{nmg-t}$ were three relevant landscape variables affecting T_{mn} . Specifically, T_{mn} was significantly and negatively correlated with W_r in summer ($r > -0.645$) ($p < 0.01$), spring ($r = -0.636$) ($p < 0.01$) and winter ($r = -0.706$) ($p < 0.01$), with the magnitude of correlation being lowest in autumn ($r = -0.366$) ($p < 0.01$). Negative correlations were observed between T_{mn} and W_{nmg-t} for summer ($r > -0.313$) ($p < 0.01$), spring ($r = -0.382$) ($p < 0.01$), autumn ($r = -0.406$) ($p < 0.01$) and winter ($r = -0.201$) ($p < 0.05$). Similarly, T_{mn} negatively correlated with $NDVI_{nmg-t}$ in summer ($r > -0.276$) ($p < 0.01$), spring ($r = -0.373$) ($p < 0.01$) and autumn ($r = -0.473$) ($p < 0.01$), but no correlation was observed in winter. Compared to W_{nmg-t} and $NDVI_{nmg-t}$, W_r was most closely and negatively associated with T_{mn} in summer, spring and winter, but it was the weakest explanatory variable in autumn. Based on scatter plots, there were obvious linear correlations between T_{mn} and W_r , W_{nmg-t} and $NDVI_{nmg-t}$ for the four seasons, except for T_{mn} and $NDVI_{nmg-t}$ in winter. In addition, some extreme values of W_{nmg-t} were observed, so discretization was applied in the modeling to reduce the overfitting problem. The seasonal correlations of the fixed river reaches were further confirmed, as significant and positive linear

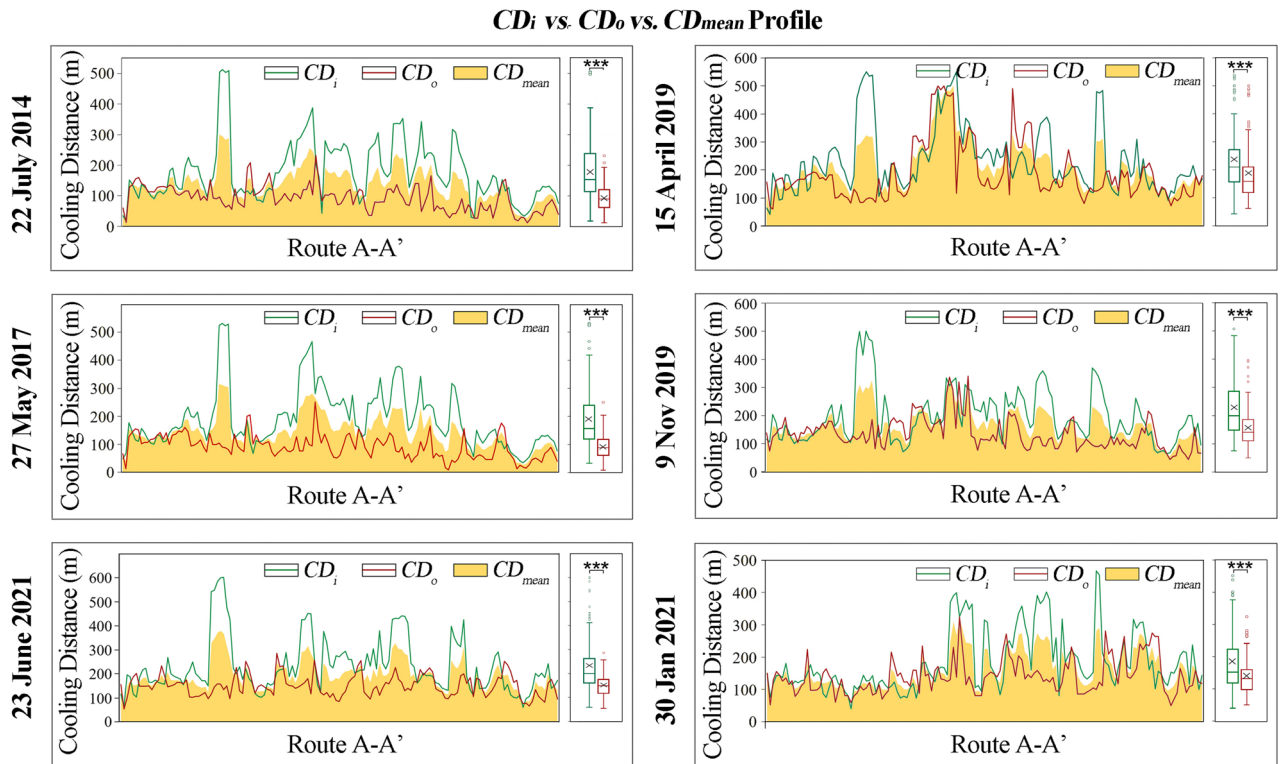


Figure 4. Profiles and distributions of cooling distances of inside (CD_i), outside (CD_o) and mean value (CD_{mean}) of 141 sampling sites along route A-A' of six dates. ***Indicate significantly different means based on an Independent-Sample t-test at 0.001 level.

correlations were observed between T_{mn} of any two of six dates, and the correlation coefficients ranged from 0.735 to 0.930 ($p < 0.01$).

Table 4 summarizes the results of the SW-MLR and RW analyses. The variance inflation factor (VIF) values ranging from 1.011 to 1.595 suggested a low level of collinearity among the explanatory variables. Overall, the results showed that W_r , W_{nng-t} and $NDVI_{nng-t}$ could explain a large amount of spatial variations in T_{mn} for all six dates (T_{mn_0722} : 69.4%; T_{mn_0527} : 67.4%; T_{mn_0623} : 74.9%; T_{mn_0415} : 73.4%; T_{mn_1109} : 54.2%; T_{mn_0130} : 56.6%) ($p < 0.001$). Specifically, the spatial variations of T_{mn} in summer, spring and autumn were mainly explained by W_r , $NDVI_{nng-t}$ and W_{nng-t} , and in winter by W_r and W_{nng-t} . The results showed that all the individual regression coefficients of the landscape variables were statistically significant ($p < 0.001$). Besides, the results indicated that W_r consistently had high values of standardized β in the different seasons. W_r consistently had the greatest explanation power of the regression models in summer (59.9%, 70.2% and 58.2%) and spring (54.9%), followed by $NDVI_{nng-t}$ and W_{nng-t} . In winter, W_r had much higher importance (88.0%) than W_{nng-t} (12.0%). The importance of W_{nng-t} and $NDVI_{nng-t}$ in explaining T_{mn} variations in autumn was noticeable compared to the other seasons.

Modelling the relationship between the maximum CD of reach and landscape indicators

The results indicated that the CD_i of 141 river reaches were significantly correlated between any two of the six dates ($p < 0.001$) (Supplementary Fig. 2). Moreover, there were positive linear correlations between the CD_i of 141 river reaches between any two of the six dates, indicating that a reach with a greater CD_i was more likely to have a greater CD_i at other times, and vice versa. In particular, correlations between winter and the other three seasons appeared lower. Similarly, the CD_o values of the fixed river sections were highly correlated between the different seasons ($p < 0.01$). However, the correlations of CD_o of 141 river reaches between different dates and seasons ($R^2 = 0.219\text{--}0.801$) ($p < 0.01$) were significantly weaker than CD_i ($R^2 = 0.391\text{--}0.907$) ($p < 0.001$).

As shown in Table 5, the VIF values ranged from 1.000 to 1.110, suggesting a low level of collinearity among the chosen landscape indicators. The results indicated that W_{nng-I} and W_{nng-O} are two dominant variables that can explain a significant portion of the spatial variations in CD_i and CD_o , respectively. Although the overall contribution of W_r to the explanatory power of the regression models was significantly smaller than that of W_{nng-I} , it was also considered a relevant explanatory factor for the variations of CD_i ($p < 0.01$) in spring and summer. The negative correlation between $NDVI_{nng-I}$ and CD_i was detected only in winter, and its contribution to the regression model (0.7%) was also significantly lower than that of W_{nng-I} (99.3%). The correlations between W_r and CD_o were found only in spring and autumn. The low importance of W_r in explaining the variations of CD_i and CD_o variations suggested that the width of a river reach might be relevant, but not important.

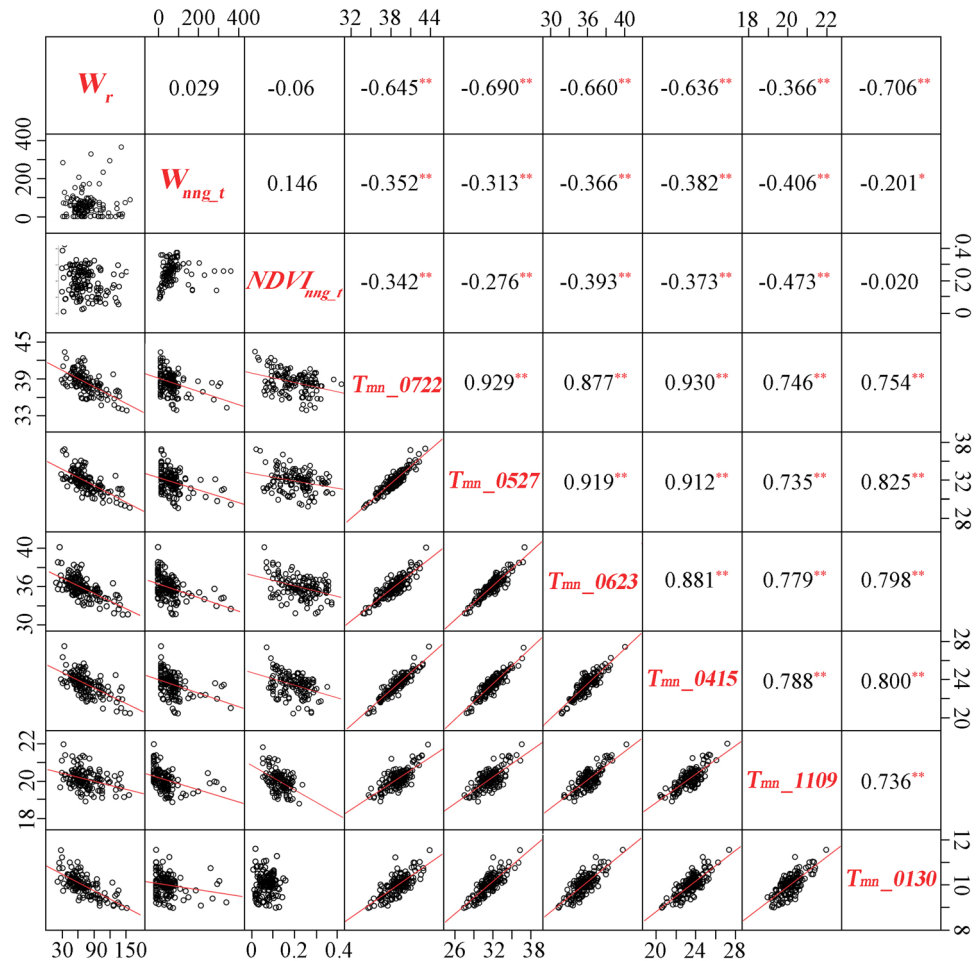


Figure 5. Relationships between landscape variables and reach LST of six dates, and seasonal correlations of LST of fixed reaches among different dates. *Significance at the 0.05 level; **Significance at the 0.01 level.

Discussion

Spatial heterogeneity of the river cooling effect and influencing factors

The results confirmed the spatial heterogeneity of LST in different sections of an urban river. Specifically, wide river sections always had a lower LST than narrow sections. The reason is that a larger water body usually has a stronger convection capacity for heat dissipation than a smaller one, which is consistent with previous studies^{30,45}. Previous studies^{27,46} indicated that the surrounding LULC of water bodies has a significant influence on UCI intensity. This study has also shown that vegetated areas have the greatest impact on UCI intensity among different LULC types along river courses in spring, summer and autumn. The presence of riverside green spaces can effectively lower the LST of the river section, as urban green spaces have been demonstrated to be another urban “cold source”^{47–49}. The coupling effect between coexisting water bodies and green spaces is still uncertain, and needs to be further investigated. The study by Wu et al.⁵⁰ found that the elevation of water bodies significantly affected the UCI intensity of water bodies. However, the elevation of river reach is not an influencing factor for LST in this study, which could be due to the narrow range of elevation data among the 141 sampling sites (3.5–5 m). Therefore, further studies should be conducted to include some regions and cities with more complex terrain conditions.

The significant differences in the cooling distances among 141 river reaches demonstrated the heterogeneity of UCI effect of an urban river in the adjacent area in all seasons, which is mainly caused by the heterogeneity of the riverbank landscape. The results of this study revealed that the cooling effect of a looping river was significantly greater on its inner side than on its outer side. The cooling distances of the different river reaches varied considerably, and ranged from 8–601 m. In particular, the correlations of CD_i ($R^2 = 0.391–0.907$) ($p < 0.001$) of fixed river sections between different dates were significantly stronger than those of CD_o ($R^2 = 0.219–0.801$) ($p < 0.01$) (Supplementary Fig. 2), suggesting that the cooling capacity of a looping river is more stable on the inner side than on the outer side.

Seasonal heterogeneity of the river cooling effect and influencing factors

The LST within a linear watercourse showed the largest fluctuations in summer, and the LST stability is strongest in winter, which is consistent with the study by Wu et al.⁵⁰. This may be due to the fact that the evaporation of

Dependent variable	SW-MLR analysis						RW analysis		
	Variables	Unstandardized coefficients		Standardized coefficients (β)	t	Sig	VIF	Raw importance	Rescaled importance (%)
		β	Std. error						
T_{mn_0722}	(Constant)	44.497	0.361		123.374	0.000			
	W_r	- 0.051	0.003	- 0.741	- 15.373	0.000	1.042	0.416	59.9
	$NDVI_{mg_t}$	- 3.771	0.619	- 0.349	- 6.089	0.000	1.469	0.231	33.3
	W_{mg_t}	- 0.276	0.060	- 0.259	- 4.580	0.000	1.427	0.047	6.8
		$R^2 = 0.694$; Adjusted $R^2 = 0.687$ Total						0.694	100.0
T_{mn_0527}	(Constant)	37.354	0.359		104.117	0.000			
	W_r	- 0.049	0.003	- 0.761	- 15.359	0.000	1.031	0.473	70.2
	$NDVI_{mg_t}$	- 5.990	1.230	- 0.282	- 4.869	0.000	1.404	0.16	23.7
	W_{mg_t}	- 0.236	0.057	- 0.238	- 4.153	0.000	1.378	0.041	6.1
		$R^2 = 0.674$; Adjusted $R^2 = 0.667$ Total						0.674	100.0
T_{mn_0623}	(Constant)	42.172	0.333		126.738	0.000			
	W_r	- 0.050	0.003	- 0.761	- 17.453	0.000	1.037	0.436	58.2
	$NDVI_{mg_t}$	- 8.614	1.120	- 0.406	- 7.690	0.000	1.524	0.278	37.1
	W_{mg_t}	- 0.228	0.052	0.228	- 4.361	0.000	1.486	0.035	4.7
		$R^2 = 0.749$; Adjusted $R^2 = 0.743$ Total						0.749	100.0
T_{mn_0415}	(Constant)	27.759	0.242		114.486	0.000			
	W_r	- 0.033	0.002	- 0.748	- 16.530	0.000	1.052	0.403	54.9
	$NDVI_{mg_t}$	- 6.571	0.987	- 0.371	- 6.656	0.000	1.595	0.278	37.9
	W_{mg_t}	- 0.194	0.037	- 0.285	- 5.224	0.000	1.535	0.053	7.2
		$R^2 = 0.734$; Adjusted $R^2 = 0.728$ Total						0.734	100.0
T_{mn_1109}	(Constant)	21.849	0.152		143.907	0.000			
	W_{mg_t}	- 0.116	0.022	- 0.369	- 5.368	0.000	1.412	0.270	49.8
	W_r	- 0.010	0.001	- 0.480	- 8.123	0.000	1.044	0.177	32.7
	$NDVI_{mg_t}$	- 5.169	0.969	- 0.372	- 5.335	0.000	1.458	0.095	17.5
		$R^2 = 0.542$; Adjusted $R^2 = 0.532$ Total						0.542	100.0
T_{mn_0130}	(Constant)	11.244	0.099		113.827	0.000			
	W_r	- 0.014	0.001	- 0.733	- 13.002	0.000	1.011	0.498	88.0
	W_{mg_t}	- 0.075	0.016	- 0.263	- 4.656	0.000	1.011	0.068	12.0
		$R^2 = 0.566$; Adjusted $R^2 = 0.560$ Total						0.566	100.0

Table 4. Results of the SW-MLR analyses and RW analyses (N = 141). T_{mn_0722} , T_{mn_0527} , T_{mn_0623} , T_{mn_0415} , T_{mn_1109} and T_{mn_0130} represent the LST of 141 sampling sites on 22 July, 2014; 27 May, 2017; 23 June, 2021; 15 April, 2019; 9 November, 2019 and 30 January, 2021, respectively.

water is highest in summer and lowest in winter. In this study, the width of the river section is the most important factor influencing LST in summer, spring and winter. In contrast, the characteristics of riverside greenspace (i.e., $NDVI_{mg_t}$ and W_{mg_t}) account for much more LST variation than the width of the river reach in autumn. This greater influence of NDVI in autumn on LST could be caused by a larger NDVI difference between 141 sampling sites, as the leaves of many deciduous tree species fall, but evergreen tree species remain standing as usual. In winter, NDVI was no longer correlated with LST, and only significant positive correlations between W_r and W_{mg_t} with LST were observed. This was mainly due to the fact that transpiration of neighboring vegetation is relatively weak in winter compared to warmer seasons. In conclusion, the relative explanatory power of these influencing factors varies with season.

Unlike the mean surface temperature, the cooling distance of a river section is more relevant to the characteristics of the adjacent green space than the scale of the reach in all four seasons. No significant correlations between the cooling distances of river reach and the NDVI values of the adjacent green spaces were observed in warm seasons. In contrast to the other seasons, the cooling distance in winter is negatively correlated with the NDVI values of the adjacent green space, suggesting that the cooling distance may be reduced with increasing vegetation density. Part of the reason may be that riverside green spaces with dense vegetation can effectively dampen the river breeze and block some winds, and therefore, reducing the cooling capacity of the river reach to the surrounding area.

Implications for urban water body design

The results demonstrated that the Outer-City River is a lower-temperature zone in four seasons. Consistent with previous studies^{30,50}, a larger river has a greater UCI intensity than a smaller one. Therefore, increasing the area of the urban water body can effectively mitigate the UHI effect. It is not an ideal method to enlarge existing water bodies from an economic and ecological point of view in highly urbanized areas. However, the amount, structure

SW-MLR analysis							RW analysis	
Dependent Variable	Variables	Unstandardized coefficients		Standardized coefficients (β)	Sig	VIF	Raw importance	Rescaled importance (%)
		β	Std. Error					
CD _i _0722	(Constant)	45.066	8.349		0.000			
	Wnng_I	0.990	0.031	0.920	0.000	1.072	0.888	99.2
	Wr	0.337	0.110	0.087	0.003	1.072	0.007	0.8
	R ² = 0.895; Adjusted R ² = 0.894 Total							0.895
CD _i _0527	(Constant)	40.344	8.622		0.000			
	Wnng_I	1.049	0.031	0.927	0.000	1.068	0.898	99.3
	Wr	0.341	0.113	0.082	0.003	1.068	0.06	0.7
	R ² = 0.904; Adjusted R ² = 0.903 Total							0.904
CD _i _0623	(Constant)	96.871	5.448		0.000			
	Wnng_I	1.077	0.018	0.972	0.000	1.057	0.965	99.8
	Wr	0.202	0.072	0.045	0.005	1.057	0.002	0.2
	R ² = 0.967; Adjusted R ² = 0.966 Total							0.967
CD _i _0415	(Constant)	86.498	9.496		0.000			
	Wnng_I	1.012	0.031	0.919	0.000	1.088	0.894	99.1
	Wr	0.429	0.127	0.094	0.001	1.088	0.008	0.9
	R ² = 0.902; Adjusted R ² = 0.901 Total							0.902
CD _i _1109	(Constant)	104.6	3.644		0.000			
	Wnng_I	1.048	0.023	0.967	0.000	1.000	0.935	100.0
	R ² = 0.935; Adjusted R ² = 0.934 Total							0.935
CD _i _0130	(Constant)	100.09	6.382		0.000			
	Wnng_I	1.076	0.032	0.946	0.000	1.002	0.887	99.3
	NDVInng_I	-168.6	59.105	-0.079	0.005	1.002	0.006	0.7
	R ² = 0.893; Adjusted R ² = 0.892 Total							0.893
CD _o _0722	(Constant)	45.502	4.253		0.000			
	Wnng_O	0.988	0.068	0.760	0.000	1.072	0.639	97.4
	NDVInng_O	55.956	21.654	0.135	0.003	1.072	0.017	2.6
	R ² = 0.656; Adjusted R ² = 0.651 Total							0.656
CD _o _0527	(Constant)	48.566	2.930		0.000			
	Wnng_O	1.024	0.054	0.851	0.000	1.000	0.724	100.0
	R ² = 0.724; Adjusted R ² = 0.722 Total							0.724
CD _o _0623	(Constant)	108.37	2.548		0.000			
	Wnng_O	1.064	0.047	0.888	0.000	1.000	0.789	100.0
	R ² = 0.789; Adjusted R ² = 0.788 Total							0.789
CD _o _0415	(Constant)	68.379	10.351		0.000			
	Wnng_O	1.329	0.052	0.886	0.000	1.110	0.842	98.8
	Wr	0.413	0.141	0.102	0.004	1.110	0.01	1.2
	R ² = 0.852; Adjusted R ² = 0.849 Total							0.852
CD _o _1109	(Constant)	83.631	6.464		0.000			
	Wnng_O	1.158	0.040	0.917	0.000	1.006	0.852	99.19
	Wr	0.215	0.081	0.085	0.009	1.006	0.007	0.81
	R ² = 0.859; Adjusted R ² = 0.857 Total							0.859
CD _o _0130	(Constant)	100.05	5.152		0.000			
	Wnng_O	1.149	0.061	0.863	0.000	1.039	0.696	97.07
	NDVInng_O	-231.3	71.803	-0.149	0.002	1.039	0.021	2.93
	R ² = 0.717; Adjusted R ² = 0.713 Total							0.717

Table 5. Results of the SW-MLR analyses and RW analyses (N = 141).

and health of the adjacent vegetation area can easily be changed and optimized through vegetation management. Thus, strategies related to increasing the area of riparian vegetated areas, increasing tree canopy cover and improving the vegetation health of adjacent green spaces are recommended. The results of this study can help to develop more specific strategies to utilize the cooling benefits of urban rivers and the riverine landscape to improve the thermal environment in urban areas.

Conclusions

In this study, the spatial heterogeneity and seasonal variation of the cooling effect of different sections of a major inner-city river in Suzhou, China, and the influencing factors were investigated and quantified. It was found that landscape indicators, including the transverse width of the river reach, the width of riverside green spaces and the NDVI of riverside green spaces, influence the magnitude of the cooling effect of different river sections in varying degrees, and together can explain a lot of the cooling heterogeneity among different river sections of the large inner-city river. The LST variations along a river are more related to its transverse width, and the variations in cooling distance are more related to the adjacent green spaces. The logarithmic relationship between LST and CD was confirmed (Supplementary Fig. 3), suggesting that the cooling distance will incline to a constant level when the LST is lower than a certain threshold, and this threshold is very close to the mean LST value of the different river sections.

The Suzhou Outer-city River in this study is just one example to demonstrate the applicability of the methodology we proposed, and more importantly, it can also be applied in other cities to quantify the cooling effect and impact factors of linear water bodies or river networks. With the increasing concern about global climate change and continued rapid urbanization, it is undoubtedly very promising to effectively utilize the combined effects of urban green space and water resources to mitigate the UHI effect through appropriate landscape strategies.

Data availability

The datasets used and analyzed in this study are available from the corresponding author upon reasonable request.

Received: 13 September 2023; Accepted: 4 April 2024

Published online: 09 April 2024

References

- Rizwan, A. M., Dennis, L. Y. C. & Liu, C. A review on the generation, determination and mitigation of Urban Heat Island. *J. Environ. Sci.* **20**, 120–128 (2008).
- Cao, C., Lee, X., Liu, S. & Schultz, N. Urban heat islands in China enhanced by haze pollution. *Nat. Commun.* **7**, 12509 (2016).
- He, B. & Zhu, J. Constructing community gardens? Residents' attitude and behaviour towards edible landscapes in emerging urban communities of China. *Urban For. Urban Green.* **34**, 154–165 (2018).
- Jin, M., Dickinson, R. E. & Zhang, D.-L. The footprint of urban areas on global climate as characterized by MODIS. *J. Clim.* **18**, 1551–1565 (2005).
- Stewart, I. D. & Oke, T. R. Local Climate Zones for Urban Temperature Studies. *Bull. Am. Meteorol. Soc.* **86**, 370–384 (2003).
- Weng, Q., Rajasekar, U. & Hu, X. Modeling urban heat islands and their relationship with impervious surface and vegetation abundance by using ASTER images. *IEEE Trans. Geosci. Remote Sens.* **49**, 4080–4089 (2011).
- Yu, Z., Yao, Y. & Yang, G. Spatiotemporal patterns and characteristics of remotely sensed regional heat islands during the rapid urbanization (1995–2015) of Southern China. *Sci. Total Environ.* **674**, 242–254 (2019).
- Voogt, J. A. & Oke, T. R. Thermal remote sensing of urban climates. *Remote Sens. Environ.* **86**, 370–384 (2003).
- Zhao, L., Lee, X., Smith, R. B. & Oleson, K. Strong contributions of local background climate to urban heat islands. *Nature* **511**, 216–219 (2014).
- Manoli, G. *et al.* Magnitude of urban heat islands largely explained by climate and population. *Nature* **573**, 55–60 (2019).
- Opdam, P., Luque, S. & Jones, K. B. Changing landscapes to accommodate for climate change impacts: A call for landscape ecology. *Landscape Ecol.* **24**, 715–721 (2009).
- Monteiro, M. V., Doick, K. J., Handley, P. & Peace, A. The impact of greenspace size on the extent of local nocturnal air temperature cooling in London. *Urban For. Urban Green.* **16**, 160–169 (2016).
- Santamouris, M., Ban-Weiss, G., Osmond, P. & Paolini, R. Progress in urban greenery mitigation science—assessment methodologies advanced technologies and impact on cities. *J. Civ. Eng. Manag.* **24**, 638–671 (2018).
- Zhou, W., Yu, W. & Wu, T. An alternative method of developing landscape strategies for urban cooling: A threshold-based perspective. *Landsc. Urban Plan.* **225**, 104449 (2022).
- Grimmond, C. S. B. & Oke, T. R. An evapotranspiration-interception model for urban areas. *Water Resour. Res.* **27**, 1739–1755 (1991).
- Manteghi, G., Limit, H. & Remaz, D. Water bodies an urban microclimate: A Review. *Mod. Appl. Sci.* <https://doi.org/10.5539/mas.v9n6p1> (2015).
- Liu, H. & Weng, Q. Seasonal variations in the relationship between landscape pattern and land surface temperature in Indianapolis. *USA. Environ. Monit. Assess.* **144**, 199–219 (2008).
- Zhao, Z.-Q., He, B.-J., Li, L.-G., Wang, H.-B. & Darko, A. Profile and concentric zonal analysis of relationships between land use/land cover and land surface temperature: Case study of Shenyang. *China. Energy Build.* **155**, 282–295 (2017).
- Spronken-Smith, R. A., Oke, T. R. & Lowry, W. P. Advection and the surface energy balance across an irrigated urban park. *Int. J. Climatol.* **20**, 1033–1047 (2000).
- Murakawa, S., Sekine, T., Narita, K. & Nishina, D. Study of the effects of a river on the thermal environment in an urban area. *Energy Build.* **16**, 993–1001 (1991).
- Cai, Z., Han, G. & Chen, M. Do water bodies play an important role in the relationship between urban form and land surface temperature? *Sustain. Cities Soc.* **39**, 487–498 (2018).
- Oliveira, S., Andrade, H. & Vaz, T. The cooling effect of green spaces as a contribution to the mitigation of urban heat: A case study in Lisbon. *Build. Environ.* <https://doi.org/10.1016/j.buildenv.2011.04.034> (2011).
- Edward, N., Chen, L., Wang, Y. & Yuan, C. A study on the cooling effects of greening in a high-density city: An experience from Hong Kong. *Build. Environ.* **47**, 256–271 (2012).
- Steenefeld, G. J., Koopmans, S., Heusinkveld, B. G. & Theeuwes, N. E. Refreshing the role of open water surfaces on mitigating the maximum urban heat island effect. *Landsc. Urban Plan.* **121**, 92–96 (2014).
- Brans, K. I., Engelen, J. M. T., Souffreau, C. & De Meester, L. Urban hot-tubs: Local urbanization has profound effects on average and extreme temperatures in ponds. *Landsc. Urban Plan.* **176**, 22–29 (2018).
- Peng, J., Jia, J., Liu, Y., Li, H. & Wu, J. Seasonal contrast of the dominant factors for spatial distribution of land surface temperature in urban areas. *Remote Sens. Environ.* **215**, 255–267 (2018).
- Du, H. *et al.* Research on the cooling island effects of water body: A case study of Shanghai. *China. Ecol. Indic.* **67**, 31–38 (2016).

28. Zhou, Y., Gao, W., Yang, C. & Shen, Y. Exploratory analysis of the influence of landscape patterns on lake cooling effect in Wuhan. *China. Urban Clim.* **39**, 100969 (2021).
29. Hathway, E. A. & Sharples, S. The interaction of rivers and urban form in mitigating the Urban Heat Island effect: A UK case study. *Build. Environ.* **58**, 14–22 (2012).
30. Syafii, N. I. *et al.* Thermal environment assessment around bodies of water in urban canyons: A scale model study. *Sustain. Cities Soc.* **34**, 79–89 (2017).
31. Wang, Y. & Ouyang, W. Investigating the heterogeneity of water cooling effect for cooler cities. *Sustain. Cities Soc.* **75**, 103281 (2021).
32. Zheng, Y., Li, Y., Hou, H. & Murayama, Y. Quantifying the cooling effect and scale of large inner-city Lakes based on landscape patterns: A case study of Hangzhou and Nanjing. *Remote Sens.* **13**, 1526 (2021).
33. Suzhou Municipal Bureau Statistics. Suzhou statistical yearbook 2021. (2022).
34. Jiménez-Muñoz, J. C., Sobrino, J. A., Skoković, D., Mattar, C. & Cristóbal, J. Land surface temperature retrieval methods from Landsat-8 thermal infrared sensor data. *IEEE Geosci. Remote Sens. Lett.* **11**, 1840–1843 (2014).
35. Cao, X., Onishi, A., Chen, J. & Imura, H. Quantifying the cool island intensity of urban parks using ASTER and IKONOS data. *Landsc. Urban Plan.* **96**, 224–231 (2010).
36. Yu, Z., Guo, X., Jørgensen, G. & Henrik, V. How can urban green spaces be planned for climate adaptation in subtropical cities?. *Ecol. Indic.* **82**, 152–162 (2017).
37. Li, Y. *et al.* Local cooling and warming effects of forests based on satellite observations. *Nat. Commun.* **6**, 6603 (2015).
38. Sun, R. & Chen, L. How can urban water bodies be designed for climate adaptation?. *Landsc. Urban Plan.* **105**, 27–33 (2012).
39. Gomez-Martinez, E., de Beurs, K. M., Koch, J. & Widener, J. Multi-Temporal Land Surface Temperature and Vegetation Greenness in Urban Green Spaces of Puebla Mexico. *Land* **10**, 1–25 (2021).
40. Zhou, W., Cao, F. & Wang, G. Effects of spatial pattern of forest vegetation on urban cooling in a compact megacity. *Forests* **10**, 282 (2019).
41. Yan, H., Wu, F. & Dong, L. Influence of a large urban park on the local urban thermal environment. *Sci. Total Environ.* **622**, 882–891 (2018).
42. Feng, W., Ding, W., Zhen, M., Zou, W. & Wang, H. Cooling effect of urban small green spaces in Qujiang Campus, Xi'an Jiaotong University. *China. Environ. Dev. Sustain.* **24**, 4278–4298 (2021).
43. Bowler, D. E., Buyung-Ali, L., Knight, T. M. & Pullin, A. S. Urban greening to cool towns and cities: A systematic review of the empirical evidence. *Landsc. Urban Plan.* **97**, 147–155 (2010).
44. Johnson, J. W. A heuristic method for estimating the relative weight of predictor variables in multiple regression. *Multivar. Behav. Res.* **35**, 1–19 (2000).
45. Amani-Beni, M., Zhang, B., Xie, G. & Xu, J. Impact of urban park's tree, grass and waterbody on microclimate in hot summer days: A case study of Olympic Park in Beijing China. *Urban For. Urban Green.* **32**, 1–6 (2018).
46. Xue, Z. *et al.* Quantifying the cooling-effects of urban and peri-urban wetlands using remote sensing data: case study of cities of Northeast China. *Landsc. Urban Plan.* **182**, 92–100 (2019).
47. Zhou, W., Yu, W., Zhang, Z., Cao, W. & Wu, T. How can urban green spaces be planned to mitigate urban heat island effect under different climatic backgrounds? A threshold-based perspective. *Sci. Total Environ.* <https://doi.org/10.1016/j.scitotenv.2023.164422> (2023).
48. Schwaab, J. *et al.* The role of urban trees in reducing land surface temperatures in European cities. *Nat. Commun.* **12**, 6763 (2021).
49. Zhang, Y., Murray, A. T. & Turner, B. L. II. Optimizing green space locations to reduce daytime and nighttime urban heat island effects in Phoenix Arizona. *Landsc. Urban Plan.* **165**, 162–171 (2017).
50. Wu, J. *et al.* Seasonal variations and main influencing factors of the water cooling islands effect in Shenzhen. *Ecol. Indic.* **117**, 106699 (2020).

Author contributions

W. Z. conceived the idea and wrote the manuscript, W. Z. and T. W. conducted the analyses, T. W. and X. T. reviewed and edited the manuscript. All authors contributed to the discussion of the results.

Funding

National Natural Science Foundation of China, 32101577, Yangzhou University, 137012167

Competing interests

The authors declare no competing interests.

Additional information

Supplementary Information The online version contains supplementary material available at <https://doi.org/10.1038/s41598-024-58879-x>.

Correspondence and requests for materials should be addressed to W.Z.

Reprints and permissions information is available at www.nature.com/reprints.

Publisher's note Springer Nature remains neutral with regard to jurisdictional claims in published maps and institutional affiliations.



Open Access This article is licensed under a Creative Commons Attribution 4.0 International License, which permits use, sharing, adaptation, distribution and reproduction in any medium or format, as long as you give appropriate credit to the original author(s) and the source, provide a link to the Creative Commons licence, and indicate if changes were made. The images or other third party material in this article are included in the article's Creative Commons licence, unless indicated otherwise in a credit line to the material. If material is not included in the article's Creative Commons licence and your intended use is not permitted by statutory regulation or exceeds the permitted use, you will need to obtain permission directly from the copyright holder. To view a copy of this licence, visit <http://creativecommons.org/licenses/by/4.0/>.

© The Author(s) 2024